Direct coordination of phenol reductants to copper enables the Cu(II) reduction in Lytic polysaccharide monooxygenases

Langxing Liao,[1,#] Jian Kuang,[2,#] Wei Peng,[3,#*] Peng Wu,[4] Xianhang Sang,[1] Heng Yin,[5] Changlin Tian[2], Lu Yu[2,*], Binju Wang[1,*]

[1]State Key Laboratory of Physical Chemistry of Solid Surfaces and Fujian Provincial Key Laboratory of Theoretical and Computational Chemistry, College of Chemistry and Chemical Engineering and Innovation Laboratory for Sciences and Technologies of Energy Materials of Fujian Province (IKKEM), Xiamen University, Xiamen 361005, P. R. China.

[2]Division of Life Sciences and Medicine, University of Science and Technology of China, Hefei 230026, P. R. China.

[3]Key Laboratory of Aerosol Chemistry and Physics, State Key Laboratory of Loess and Quaternary Geology (SKLLQG), Institute of Earth Environment, Chinese Academy of Sciences, Xi'an 710061, P. R. China.

[4]State Key Laboratory of High-Efficiency Utilization of Coal and Green Chemical Engineering, School of Chemistry and Chemical Engineering, Ningxia University, Yinchuan 750021, P. R. China.

[5]Dalian Engineering Research Center for Carbohydrate Agricultural Preparations, Dalian Technology Innovation Center for Green Agriculture, Liaoning Provincial Key Laboratory of Carbohydrates, Dalian Institute of Chemical Physics, Chinese Academy of Sciences, Dalian 116023, P. R. China.

***KEYWORDS**: Phenol-mediated Cu(II) reduction, Lytic polysaccharide monooxygenases, particulate methane monooxygenase, Frontier orbital energies, QM/MM*

ABSTRACT: Copper-dependent lytic polysaccharide monooxygenases (LPMOs) are key enzymes involved in the breakdown of recalcitrant polysaccharides such as cellulose and chitin. LPMOs require external electrons for the activations of either O_2 or H_2O_2, which can be supplied by enzymatic electron donors or small molecule reductants. As quite abundant reductants in nature, phenolic compounds can serve as efficient reducing agents for reactions of LPMOs. Despite extensive studies, how phenolic compounds fuel the reactions of LPMOs is enigmatic. In this study, we report a novel mechanism for the reduction of LPMO-Cu(II) by the phenol reductants. Among various mechanisms investigated, we found the most favorable one involves the coordination replacement of water by the phenol reductant. The coordination of pyrogallol (Pyr) to LPMO-Cu(II) can remarkably facilitate both the electron transfer from Pyr to Cu(II) and the proton transfer from the ligated OH group to the adjacent Glu148, thereby enhancing proton-coupled electron transfer process for the reduction of LPMO-Cu(II). Detailed comparisons and analysis have shown that the different ligand effects between LPMOs and the copper-dependent pMMO can result in the divergent mechanisms for Cu(II) reduction in two enzymes. These insights have greatly expanded our understanding on the interaction machinery of copper-dependent enzymes with phenol compounds in nature.

INTRODUCTION: Lytic polysaccharide monooxygenases (LPMOs) are the representative copper-dependent enzyme family that play a critical role in the degradation of polysaccharides, particularly in the breakdown of recalcitrant polysaccharides such as cellulose and chitin.[1-11] Structurally, LPMO retains the conserved histidine brace motif at the active site, where the mononuclear copper is ligated to three N sites of two histidine residues (Figure 1A and 1B).[6, 12-16] LPMOs were initially identified to be O_2-dependent oxidases, which can mediate the C−H (BDE=95 kcal/mol) hydroxylation of polysaccharides via the external reductant-assisted oxygen activation process (Figure 1A).[17-21] In addition, it was found that LPMOs can use the H_2O_2 co-substrate to perform preoxygenations on polysaccharides, for which the pre-activation of LPMOs by an external reducing agent is required.[13, 22-25] Interestingly, O_2-dependent activity of LPMOs can generate the H_2O_2 intermediate in the presence of reducing agent (e.g. ascorbate),[26-31] suggesting the O_2-dependent pathway and the H_2O_2-dependent pathway are connected by the H_2O_2 intermediate. Due to the oxidizing power of LPMOs,

extensive interests have been devoted to their catalytic functions, including the biomass conversion and degradation, biorefinery and waste processing. [4, 7, 32-33]

For either O_2 or H_2O_2-dependent pathways, the electron input is required to fuel the reactions of LPMOs.[34] The mostly widely used electron donors include either small molecule reductants, or the typical enzymatic electron donors such as cellobiose dehydrogenase (CDH).[35-39] In terms of small molecule reductants, ascorbic acid (Asc) has been extensively used for LPMO assay. As a strong reductant, Asc can efficiently reduce LPMO-Cu(II) to LPMO-Cu(I), [40-41] thereby facilitating the following O_2 or H_2O_2 activations. In addition to Asc, various diphenol and triphenol compounds are found to be serves as reducing agents for reactions of LPMOs (Figure 1C).[35-36] In particular, the catalytic efficiency of LPMOs with phenol reductants can be even higher than that with Asc.[36] As phenolic compounds are quite abundant in nature and can be sourced from various plants, microorganisms and lignin,[35] they may function as ubiquitous reductants for the actions of LPMOs and other copper-dependent enzymes.[42]

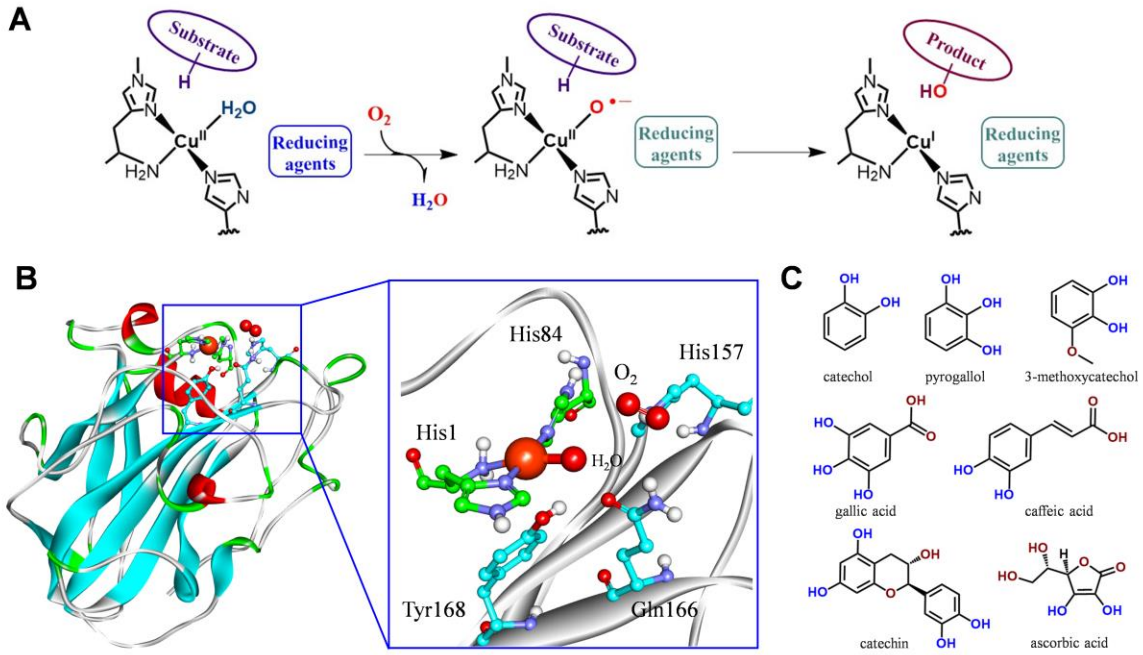

Figure 1. (A) Possible reaction mechanism of LPMOs in the presence of O_2 and external reductants. (B) Crystal structure of AA9 LPMO from *Neurospora Crassa* (PDB code 5TKG[43]), the resting state of LPMO's Cu(II) is coordinated by His1, His84 and water molecule, while O_2 is bound near His157. (C) Various phenol reductants for reactions of LPMOs, while ascorbic acid is the one of widely used small-molecule reductants in LPMO assays.

Despite their important roles for the activations of LPMOs, how phenolic compounds fuel the reactions of LPMOs are still enigmatic up to now. Unlike Asc, phenolic compounds are generally poor one-electron donor for the reduction of Cu(II), so it is unknown how LPMO-Cu(II) can be reduced by phenolic reductants. Finally, it is intriguing to compare the activation mechanism of LPMOs vs. the Cu_D site of pMMO. As both mononuclear copper-dependent enzymes can employ diphenol compounds as their reducing agents.[36, 44-48] *Understanding the ligand effects and the actions of phenol reductants are definitely beneficial for the development of LPMO-inspired synthetic catalysts.*

To address the above emerging issues in LPMOs, the combined molecular dynamics (MD) simulation, quantum mechanics/molecular mechanics (QM/MM) calculations, spectroscopy and mutagenesis studies have been conducted. Unlike Asc, our study show the triphenol reductant pyrogallol (Pyr) is not able to reduce LPMO-Cu(II) via direct electron transfer. Instead, our study reveals that the LPMO-Cu(II) reduction requires the direct coordination of phenol reductant to Cu center, through which the reduction of the LPMO-Cu(II) can be achieved via a PCET mechanism. The reduction of LPMO-Cu(II) has been supported by electron paramagnetic resonance (EPR) results. Detailed comparisons and analysis have shown that the different ligand effects between LPMOs and the copper-dependent pMMO can result in the divergent mechanisms for Cu(II) reduction in two enzymes. These findings have far-reaching implications on both the copper catalysis and functional machinery of phenol compounds in nature.

METHODS:

System setup. The initial 3D structures were prepared as follows: the structure of *Ls*AA9A LPMO (CAZy classification AA9) was based on the X-ray structure from *Aspergillus oryzae* fungus (PDB code: 5ACI),[6] and the structure of pMMO was prepared by the cryo-EM structure, which come from *Methylococcus capsulatus* str. Bath bacterium (Protein Data Bank code: 8OYI).[47] Firstly, three titratable residues in LPMO and pMMO were assigned to rational protonation states based on p*K*a determined using PROPKA software[49] and a comprehensive visual

assessment of local H-bond networks. In LPMO, the histidine residues (No. 66, 78, 79, 125 and 131) were protonated at the δ position, while His147 was protonated at the ε position. For His122, it was doubly protonated. The N-terminal His1 is an ε-methylated histidine that coordinates the metal ion through its imidazole Nδ and amino-terminal NH_2. All glutamate and aspartate residues were deprotonated. For the protonation states in pMMO, histidine residues No. 139 and 307 in PmoB, No. 11, 40, 168 and 232 in PmoA, No. 134, 160, 173, 231 (812) and 245 (826) in PmoC were protonated at the δ position, while for No. 33, 48, 72, 137, 192 in PmoB and 38 in PmoA, they were protonated at the ε position. For glutamate and aspartate residues, except glutamate residues No. 96, 100 and 176 in PmoC, which were protonated, the remaining residues were deprotonated. Subsequently, the missing hydrogen atoms of the protein residues were completed using the LEAP module in Amber18.[50]

The semi-flexible docking module of AutoDock was utilized to dock the reducing cofactors Pyr and DQH_2 to the Cu(II) catalytic centers of LPMO and pMMO, respectively. The MCPB.py module[51] was used to parameterize the force field for the initial resting-state active centers (Cu(II) coordination sphere in LPMO and Cu_D(II) coordination sphere in pMMO). The AMBER GAFF[52] force field was applied to Pyr and DQH_2, with partial atomic charges derived from RESP models[53] calculated at the HF/def2-SVP theoretical level. The classic amber force field ff14SB was used for the all of the amino acids. To neutralize the system, 9 Na^+ ions were added to the LPMO protein surface and 8 Na^+ ions to the pMMO protein surface. Each system was then immersed in a rectangular box of TIP3P water molecules, extending at least 15 Å from the surfaces of LPMO and pMMO. Comprehensive 100 ns MD simulations were performed for each system. Further details on MD and QM/MM MD simulations are provided in the *SI Appendix*.

QM/MM simulations. The final snapshot from the QM/MM MD trajectories was selected as the starting point for the QM/MM calculations. These calculations were performed with ChemShell,[54-55] integrating Turbomole[56] for the QM region and DL_POLY[57] for the MM region. In order to take into account for the polarizing effect of the protein environment on the QM regions, the electrostatic embedding scheme was applied.[58] Hydrogen link atoms and the charge-shift model were employed to manage the QM/MM boundary. For the geometry optimization of the QM regions, they were carried out by using the hybrid UB3LYP density functional[59-61] with a double-ζ basis set def2-SVP, while energy refinements utilized the larger def2-TZVP basis set. Dispersion corrections were included using Grimme's D3 method.[62-64] Transition states (TSs) were identified along the reaction coordinates by pinpointing the highest points on the potential energy surface, with a scanning increment of 0.02 Å. TSs were located from finely scanned energy surfaces, and all minima were optimized without symmetry constraints using the DL-FIND optimizer.[65] The amino acids in the MM region were treated using the Amber ff14SB force field,[66] while water molecules were modeled with the TIP3P force field. For the stage of LPMO-Cu(II) reduction, the QM region included the reducing agent Pyr, the copper atom, the coordinated residues His1 and His78, and a water molecule. Additionally, Glu148, and Tyr164 were included. For the Cu(II) reduction process in pMMO, the QM region encompassed the reducing agent DQH_2, the copper atom, coordinated residues Asn227, His231, His245, and a water molecule, with Glu228 included as the proton acceptor. The relative energies computed were electronic energies from the QM/MM calculations. Previous studies on metalloenzymes have shown that the electronic energy barrier serves as a reliable approximation of the free energy barrier.[67-78]

DFT calculations. DFT calculations of Cu(II)−H_2O---Pyr^-, Cu(II)−Pyr^- and Cu_D(II)−H_2O---DQH^- were performed in ORCA (version 5.0.3)[79] with the functionals B3LYP and the basis set def2-SVP. Molecular orbitals were calculated in ORCA with the same B3LYP/def2-SVP and visualized in VMD[80] and Multiwfn.[81]

Cloning and expression of *Ls*AA9A. The gene encoding *Ls*AA9A (GenBank ALN96977.1, amino acid sequence was described in SI) was synthetized after codon optimization for *P. pastoris* (GenScript, Nanjing, China) and inserted into the vector pPICZαA with the C-terminal $(His)_6$-tag. The pPICZαA-*Ls*AA9A plasmid was linearized with *Pme I* (NEB, USA), and then was transformed into *P. pastoris* X33 by using electroporation as described.[82] The recombination X33 strain containing Zeocin resistant were screened for protein production.[82] The cells were grown in 100 ml BMGY medium (1% (w/v) yeast extract, 2% (w/v) peptone, 1.34% (w/v) YNB, 4×10^{-5}% (w/v) biotin, 1% (v/v) glycerol, and 100 mM potassium phosphate, pH 6.0) at 28 °C for 16 h until the absorbance of 600 nm was at ~ 2 to 6. The cells were pelleted by centrifugation and resuspended in 400 ml BMMY medium (1% v/v methanol replaced 1% v/v glycerol in BMGY) at 25 °C. The methanol was added to inducible expression for 5 days with 1% (v/v) per day. The culture supernatants were collected using centrifugation and filtered through 0.22 μm filters (Sangon Biotech, Shanghai, China).

Purification and copper loading of *Ls*AA9A. The AKTAxpress system (GE healthcare) was used for Purification of protein. The supernatants were was added to 5 mL His-Trap column (GE Healthcare) which pre-equilibrated with 20 mM Na_3PO_4, 500 mM NaCl, and 20 mM imidazole, pH 7.4 (binding buffer), and the column was equilibrated by binding buffer. The proteins were eluted by eluting buffer (20 mM Na_3PO_4, 500 mM NaCl, and 500 mM imidazole, pH 7.4). Target proteins were desalted by loading onto a PD-10 column (PD SpinTrap G-25, Cytiva) and buffer exchanged in 50 mM ammonium acetate buffer, pH 6.0. The protein concentrations were determined using a modified Bradford Protein Assay Kit (Sangon Biotech, Shanghai, China) and analyzed by SDS-PAGE. *Ls*AA9A was incubated with 5-fold $CuSO_4$ at 4 °C for 16 h. Excess of copper was removed by using PD-10 column in 50 mM ammonium acetate buffer, pH 6.0 and proteins were concentrated with a 10

kD Ultrafiltration centrifugal filters (Merck Millipore).

Phenol reductants oxidation assay. Samples containing 1 μM *Ls*AA9A, water or $CuSO_4$ were incubated with 100 μM phenol reductants in 50 mM sodium phosphate buffer, pH 6.0, at 30 ℃ for an hour, according to a previous report.[83] The oxidation of phenol reductants was measured at 325 nm band. The different buffer including 50 mM ammonium acetate (pH 6.0), 50 mM Tris-HCl (pH 7.4), 100 mM KPi (pH 8.0) or water was incubated with 1 mM Pyr at 30 ℃ for an hour, respectively.

Electron paramagnetic resonance (EPR) measurements. All samples for EPR spectroscopy were prepared in an anaerobic glove box (96% N_2/4% H_2, Coy Laboratory Products, USA). All materials were subjected to thorough degassing and incubated in the anaerobic glove box for at least 12 hours prior to use. For all samples, glycerol (10% v/v) was added as a cryoprotectant. For the preparation of Pyr-reduced protein samples, LPMO was incubated with a freshly prepared Pyr solution and excess Pyr was removed using a desalting column (PD SpinTrap G-25, Cytiva). The resulting mixture was transferred to quartz EPR tubes (707-SQ-250 M, 4 mm O.D., Wilmad), sealed, and removed from the anaerobic environment. Samples were immediately flash-frozen and stored in liquid nitrogen until experiment. The Pyr-reduced samples were further re-oxidized by either being exposed to air or treated with iodosobenzene (PhIO).

Low-temperature EPR experiments were performed using a Bruker A300 spectrometer (Bruker Biospin GmbH, Rheinstetten, Germany) equipped with a high-sensitivity cavity (ER4119HS, Bruker Biospin GmbH, Rheinstetten, Germany). Sample temperature was maintained at 120 K using a liquid nitrogen finger dewar insert and a Bruker variable temperature control unit. EPR parameters were as follows: microwave frequency, 9.447 GHz; microwave power, 10 mW; modulation frequency, 100 kHz; modulation amplitude, 10.00 G; time constant, 163.84 ms; conversion time, 16.00 ms. Typically, 10 scans were performed for each sample to ensure a reliable signal-to-noise ratio. EPR spectral simulations were performed using the EasySpin (Version 5.2) toolbox operating in the Mathworks MATLAB environment.[84] Parameters for the simulations were summarized in Figure S1.

RESULTS & DISCUSSION:

O_2 reduction mechanism in LPMO: role of direct coordination of Pyr to Cu(II). In LPMOs, it was found both experimentally and computationally that the reductant Asc can efficiently reduce Cu(II) to Cu(I).[7, 37, 85] Then, the Cu(I) can bind oxygen molecule and mediate the following the oxygen activation.[34, 85-87] In terms of phenol reductant Pyr, the MD and QM/MM MD show that the reductant Pyr can be anchored by hydrogen bond interactions with Glu148, the Cu(II)-coordinated H_2O and His147 (Figure S2). Starting from such reactant (RC), we first gauged various mechanisms for the reduction of LPMO-Cu(II). The first one (Figure 2B) involves the direct electron transfer (ET) from Pyr to the Cu(II) center. Since a spontaneous ET from Pyr to Cu(II) was not observed in the QM/MM-optimized RC, we have assessed the energetics of such ET with QM model calculations. As shown in Figure 2B, the ET process is endothermic by 15.0 kcal/mol, indicating the one-electron reduction of Cu(II) via the direct ET is highly unfavorable in LPMO. The second mechanism involves a PCET process (Figure 2C), which was also considered in pMMO.[48] In such a PCET mechanism, the proton transfer (PT) from hydroxyl group in Pyr to Glu48 may drive the ET from Pyr to Cu(II). However, our QM data show that such process is endothermic by 18.7 kcal/mol, indicating the directly PCET is still highly unfavorable. This is mainly because that the Cu(II) center maintains a highly saturated coordination architecture, thereby leading to the significant reduction of the redox-potential of Cu(II) for the electron acceptation. Obviously, the phenol mediated LPMO-Cu(II) reduction should differ from the one mediated by Asc.

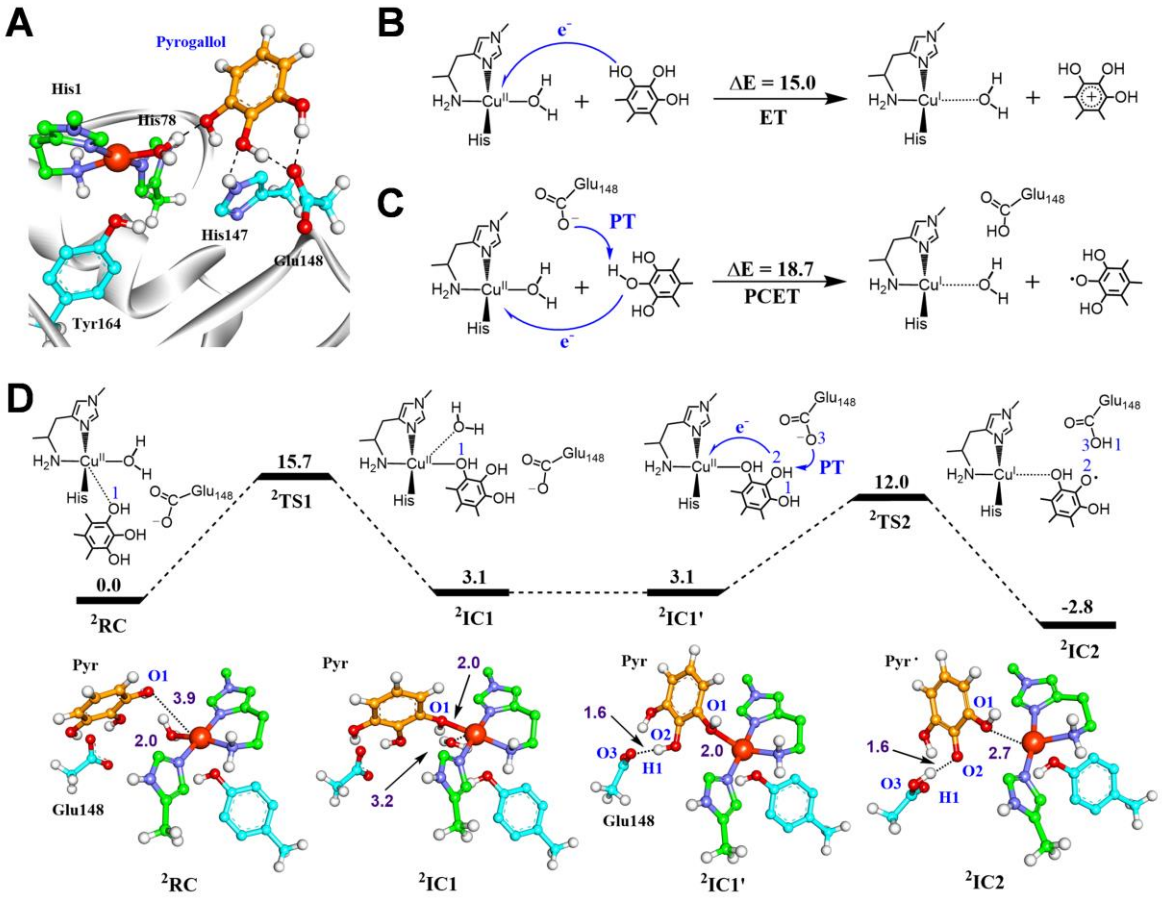

Figure 2. Possible mechanisms for reduction of the Cu(II) site by the reductant Pyr. (A) The QM/MM MD equilibrated geometry of the binding conformation of Pyr in *Ls*AA9 LPMO. (B) QM(UB3LYP-D3/def2-TZVP) relative energies (kcal/mol) for one-electron reduction of Cu(II) to Cu(I). (C) QM(UB3LYP-D3/def2-TZVP) relative energies (kcal/mol) for the PCET-mediated reduction of Cu(II) to Cu(I). (D) QM(UB3LYP-D3/def2-TZVP)/MM relative energies (kcal/mol) for the coordination of Pyr to Cu(II) enables PCET to afford the Cu(I) intermediate (^{2}IC2). Key distances are given in Å unit.

As the direct ET and PCET mechanism can be excluded for the Cu(II) reduction, we assume that the phenol OH group may displace the equatorial H_2O and coordinate to Cu(II) directly. Figure 2D presents the QM/MM energy profile for the Cu(II) reduction via the Pyr-coordination mechanism. It is seen that the coordination of Pyr-O1 to Cu(II) drives the dissociation of equatorial H_2O, leading to the Pyr-ligated IC1 that is 3.1 kcal/mol higher than RC. The process should overcome a barrier of 15.7 kcal/mol. Starting from IC1, we investigated the Cu(II) reduction via a possible PCET mechanism, during which the proton transfer from Pyr-O2 to Glu148 is coupled to the electron transfer from Pyr to Cu(II). However, the process requires a relatively high energy barrier of 17.3 kcal/mol relative to IC1 (see Figure S3), possibly due to the unfavorable Cu(II)'s coordination environment in IC1, where a water is anchored by the H-bond interaction with Pyr-OH group and weakly coordinated to Cu(II) (Cu-O_{WAT} distance: 2.25 Å). Such coordination pattern may impede the reduction of Cu(II) by Pyr. To probe the possible coordination reorganization of Cu(II), MD simulation was performed on IC1. As shown in Figure 2D, the Tyr-OH group can reorient during the MD and lead to the disruption of H-bond interaction with water and then the dissociation of water from Cu(II) in IC1'. Due to the dissociation of the axial water, the Cu(II) reduction by Pyr can be facilitated. Such machinery is analogous to the case of P450s.[88-91] Starting from IC1', the following Cu(II) reduction via the PCET mechanism was found to be facile with a small energy barrier of 8.9 kcal/mol (IC1'→TS2, Figure 2D and S4). The process affords the reduced Cu(I) along with the Pyr radical in IC2, as confirmed by the spin-density population of 0.01 at Cu center and 0.97 at Pyr, respectively. In IC2, we can see that the Pyr radical is dissociated from Cu(I), with a Cu−O1 distance of 2.7Å, which basically aligns with a low-coordination nature of Cu(I) as observed in pMMO.[45, 48] *Thus, our simulations enable us to identify a phenol-coordination mechanism for LPMO-Cu(II) reduction, which was unexpected before*.

Spectroscopic determination of Cu(II) reduction. To gain insights into the reduction of LPMO-Cu(II) by Pyr, we conducted X-band continuous-wave EPR spectroscopy experiments. These experiments were designed to explore the signal characteristics of Cu(II) before and after the interaction of *Ls*AA9A LPMO with Pyr. As illustrated in Figure 3, in the absence of

Pyr, the X-band EPR spectrum exhibited a prominent signal originating from the Cu(II) site (depicted in black, Figure 3A). The predominant rhombic signal arises from a type-2 Cu(II) center characterized by a rhombic g-tensor of [2.061, 2.060, 2.280] with hyperfine splitting parameters associated with the extensively studied Cu(II) site[92-94] (A_{ZZ} = 530 MHz) according to spectral simulations (Figure S1).

Under anaerobic conditions, upon introduction of 5-fold Pyr, a notable reduction in the Cu(II) signal is accompanied by conspicuous superhyperfine splittings originating from neighboring nitrogen atoms (orange, Figure 3A). Concurrently, the mixture undergoes a color transformation from colorless to yellow-brown, attributed to the oxidation of Pyr.[95-96] Upon further addition of 20-fold Pyr, the Cu(II) signal nearly disappears (red, Figure 3A), resembling the case where the Asc reductant is employed in the reaction (Figure S5), in which the complete elimination of the Cu(II) signal is observed. This indicates Pyr's efficacy in reducing Cu(II) to Cu(I). Once the system was exposed to air for 10 minutes, we can observe a rapid increase in the Cu(II) signal (blue, Figure 3B), akin to the signal intensity observed upon air exposure in the *Ls*AA9A LPMO-Asc reaction system (Figure S5). This suggests that the further oxidation of Cu(I) by O_2 can lead to Cu(II) again. Subsequent addition of excess iodosobenzene (PhIO) results in a more pronounced intensification of the Cu(II) signal in the *Ls*AA9A LPMO-Pyr mixture system (green, Figure 3B), confirming that Pyr can indeed reduce the *Ls*AA9A LPMO.

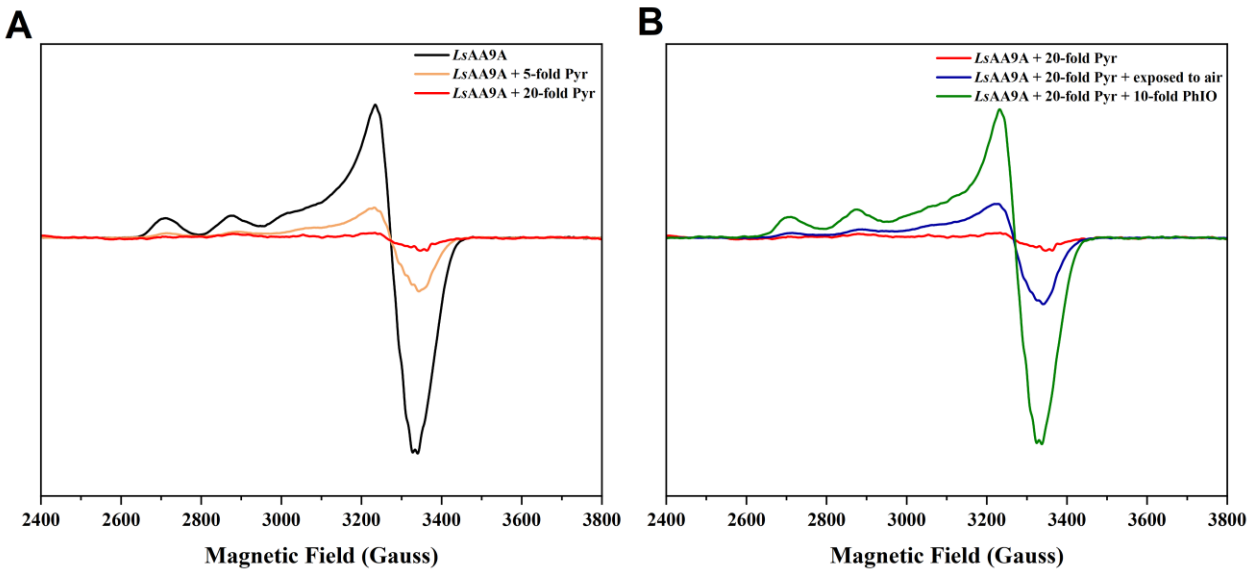

Figure 3. EPR spectroscopic characterization of *Ls*AA9A LPMO under different redox conditions. (A) EPR spectra of *Ls*AA9A LPMO as in oxidized state and in reduced state by treated with different equivalents of Pyr. (B) EPR spectra of *Ls*AA9A LPMO as in Pyr-reduced state and in re-oxidized state following either exposure to air or treatment with PhIO.

Why the phenol coordination is required for LPMO-Cu(II) reduction? As shown in former sections, the reduction of LPMO-Cu(II) requires a priming coordination of Pyr to Cu(II). So, the left question is why the LPMO-Cu(II) reduction can only be achieved by the Pyr coordination, rather than the outer sphere ET from the phenol reductant. To answer this question, we first evaluated the proton-donating ability (acidity) of phenol OH group in Cu(II)−H_2O---Pyr vs. Cu(II)−Pyr. QM calculations indicated that the energy required for removing the proton from the phenol OH group can decrease by 22.4 kcal/mol upon the Pyr coordination to Cu(II) (Figure S6), indicating that Pyr coordination can greatly enhance the proton donating ability/acidity of the phenol OH group. Second, we have analyzed the frontier orbitals in the Cu(II)−H_2O---Pyr vs. Cu(II)−Pyr systems. As the PCET process involves the electron transfer from the highest occupied molecular orbital (HOMO) of phenol fragment to the lowest unoccupied molecular orbital (LUMO) of Cu, we have plotted the energy level of these two key orbitals in Figure 4. In the H_2O-coordinated system (Figure 4A), the HOMO mainly consists of the bonding π orbital of Pyr^- (52% from Pyr^- and 34% from copper), while the LUMO is primarily composed of the anti-bonding orbital of Cu d_{x2-y2} (59% from copper and 12% from Pyr^-). It is seen that the energy gap of these two orbitals is 1.4 eV. As for the Pyr-ligated system, the MO diagram of Cu(II)−Pyr^- (Figure 4B) shows that the HOMO mainly consists of the π orbital of Pyr^- (65% from Pyr^- and 26% from copper), whereas the LUMO is composed of the anti-bonding orbitals from both Cu d_{x2-y2} and Pyr^- (45% from copper and 38% from Pyr^-). In addition, we can see that the energy gap between HOMO and LUMO orbital of σ* has been reduced to 0.32 eV, suggesting that the ET process can be significantly enhanced in the Pyr-ligated system. *Thus, our analysis show that the Pyr-ligation can remarkably facilitate both the ET and PT*

processes, thereby enhancing the PCET process for the LPMO-Cu(II) reduction.

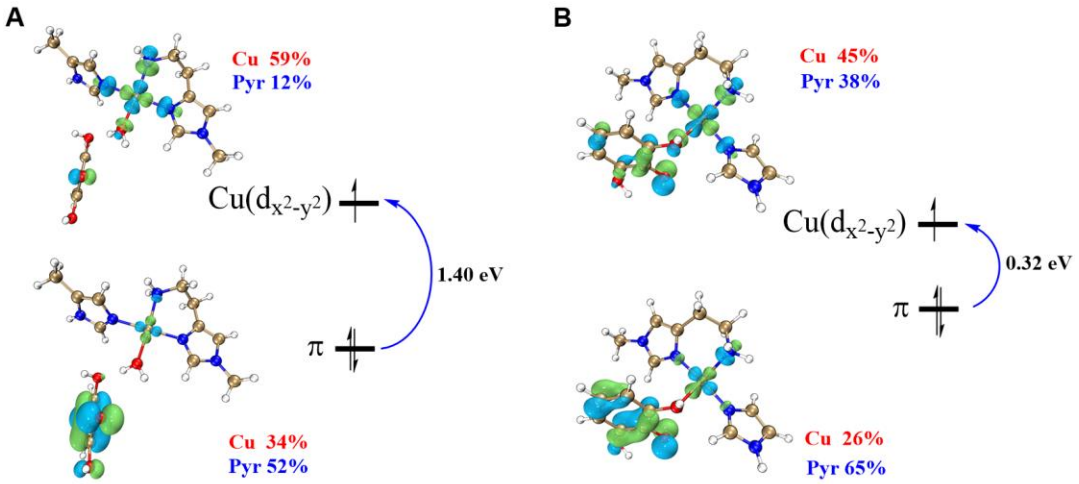

Figure 4. The frontier orbital energies of the LPMO active site in the presence of the reductant Pyr. (A) Cu(II)−H_2O---Pyr^- complex; (B) Cu(II)−Pyr^- coordination states.

Cu(II) reduction occurs via the divergent mechanisms between LPMO and pMMO. Since both LPMO and pMMO are mononuclear copper enzymes, it is interesting to compare if both enzymes employ the same or different mechanisms for the Cu(II) reduction. In pMMO, recent experimental and computational evidences show that the Cu_D(II) center is the active site for oxygen activation and methane oxidation (recently identified as the methane oxidation center) in pMMO.[44, 97] For the Cu_D(II) reduction by the phenolic reductant duroquinol (DQH_2) in pMMO, our QM/MM calculations show that the PT to Glu809 drives ET to Cu_D(II), which involves a small energy barrier of 11.0 kcal/mol and an exothermicity of 0.6 kcal/mol (RC_{CuD}→$IC1_{CuD}$, Figure 5B and S7). Obviously, the phenol reductant can reduce the Cu_D(II) via a direct PCET mechanism in pMMO, which differs from the situation of LPMO, where the phenol coordination is required for LPMO-Cu(II) reduction.

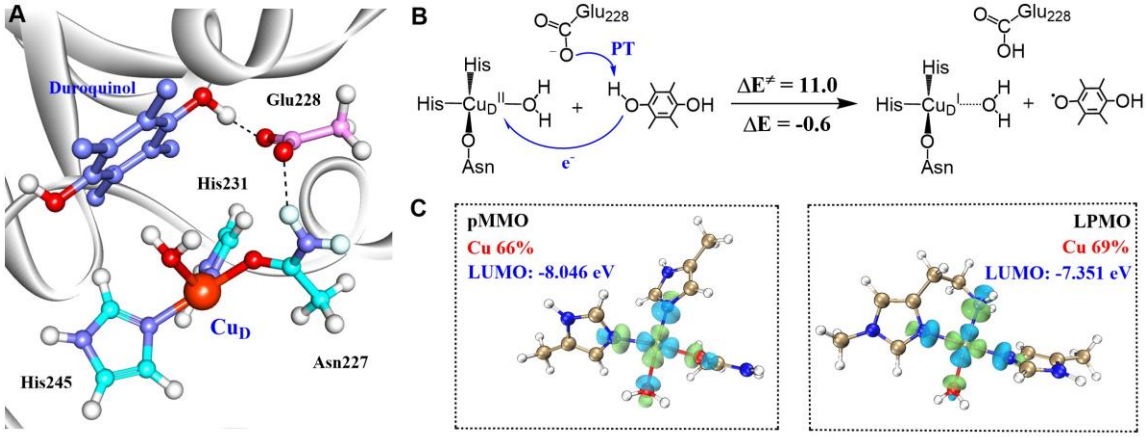

Figure 5. The QM/MM calculated mechanism for the reduction of pMMO Cu_D(II) by DQH_2. (A) The QM/MM MD equilibrated geometry of the binding conformation of DQH_2 in pMMO. (B) QM(UB3LYP-D3/def2-TZVP)/MM relative energies (kcal/mol) for the Glu809 mediated direct PCET to afford the Cu_D(I) intermediate in pMMO. (C) The LUMO orbital energy of resting state Cu(II)−H_2O in pMMO and LPMO. Key distances are given in Å unit.

To get some clues about the divergent mechanisms of Cu(II) reduction in LPMO vs. pMMO, we have computed the bond dissociation energies (BDE) of the phenols' O−H bonds and the electron affinity of Cu(II) center for both enzymes. For the BDE of the two phenols' O−H bonds, the calculated values are 66.2 kcal/mol for DQH_2 (for pMMO), and 64.2 kcal/mol for the middle OH group of Pyr (for LPMO). This indicates that Pyr is even more redox-active than DQH_2, suggesting that the BDE of the

different phenols' O−H bonds is not the key determinant for the divergent mechanisms in LPMO vs. pMMO. Thus, we further gauged the electron-accepting ability of the Cu(II) active site for both enzymes. As shown in Figure 5C, the LUMO orbital energy of the pMMO-Cu_D(II) active site (66% from copper) is -8.05 eV, whereas the LUMO orbital energy of the LPMO-Cu(II) active site (69% from copper) is -7.35 eV. This indicates that the pMMO-Cu_D(II) site has much higher capability to accept the electron from the phenol reductant than that of LPMO-Cu(II). Inspection of the active site structure (Figure 1B) shows that the LPMO-Cu(II) is strongly coordinated by a deprotonated -NH_2 group, whereas pMMO-Cu_D(II) is loosely coordinated by the carbonyl group of Asn227. *Compared to pMMO-Cu_D(II), the stronger ligand effect in LPMO-Cu(II) elevates the energy level of frontier orbitals, thereby reducing the electron accepting ability of LPMO-Cu(II) for the PCET reaction* (Figure S8).

CONCLUSIONS:

In this study, we have uncovered a novel mechanism for the reduction of LPMO-Cu(II) by the phenol cosubstrate Pyr. Among various mechanisms investigated in this study, we noticed the most favorable pathway is the coordination replacement of water by the Pyr reductant. The coordination of Pyr to LPMO-Cu(II) can remarkably facilitate both the electron transfer from Pyr to Cu(II) and the proton transfer from the ligated OH group to the adjacent Glu148, thereby enhancing the PCET process for the LPMO-Cu(II) reduction. The reduction of LPMO-Cu(II) by Pyr was confirmed by EPR experiments, wherein the addition of Pyr results in a notable decrease in the Cu(II) EPR signal. Thus, our study shows that the catalytic site architecture of LPMO is key to the productive binding of phenol reductants, suggesting that phenol compound may function as key reductants for the activation of LPMO. Unlike LPMO, we found that the weak ligand effects in Cu_D site of pMMO can significantly elevate the redox-potential of pMMO-Cu_D(II) site, thereby rendering a different mechanism for pMMO-Cu_D(II) reduction, as compared to the LPMO-Cu(II) counterpart. All these insights have greatly expanded our understanding on the phenol-reductant-mediated LPMO catalysis, as well as the ligand effects in modulating the reactivity of copper active site.

ASSOCIATED CONTENT

Supporting information

The EPR spectra, MD, QM/MM MD simulation results, QM and QM/MM energies, as well as the Cartesian coordinates and Mulliken spin density of all computed species.

AUTHOR INFORMATION

Corresponding Authors

Wei Peng: − *Key Laboratory of Aerosol Chemistry and Physics, State Key Laboratory of Loess and Quaternary Geology (SKLLQG), Institute of Earth Environment, Chinese Academy of Sciences, Xi'an 710061, P. R. China;* orcid.org/0000-0002-4085-5842; Email: weipeng@cau.edu.cn

Lu Yu: − *Division of Life Sciences and Medicine, University of Science and Technology of China, Hefei 230026, P. R. China;* orcid.org/0000-0003-4852-0008; Email: luyuesr@ustc.edu.cn

Binju Wang: − *State Key Laboratory of Physical Chemistry of Solid Surfaces and Fujian Provincial Key Laboratory of Theoretical and Computational Chemistry, College of Chemistry and Chemical Engineering and Innovation Laboratory for Sciences and Technologies of Energy Materials of Fujian Province (IKKEM), Xiamen University, Xiamen 361005, P. R. China;* orcid.org/0000-0002-3353-9411; Email: wangbinju2018@xmu.edu.cn

Authors

Langxing Liao: − *State Key Laboratory of Physical Chemistry of Solid Surfaces and Fujian Provincial Key Laboratory of Theoretical and Computational Chemistry, College of Chemistry and Chemical Engineering and Innovation Laboratory for Sciences and Technologies of Energy Materials of Fujian Province (IKKEM), Xiamen University, Xiamen 361005, P. R. China.*

Jian Kuang: −*Division of Life Sciences and Medicine, University of Science and Technology of China, Hefei 230026, P. R. China.*

Peng Wu: − S*tate Key Laboratory of High-Efficiency Utilization of Coal and Green Chemical Engineering, School of Chemistry and Chemical Engineering, Ningxia University, Yinchuan 750021, P. R. China;* orcid.org/0009-0008-5472-5847

Xianhang Sang: − *State Key Laboratory of Physical Chemistry of Solid Surfaces and Fujian Provincial Key Laboratory of Theoretical and Computational Chemistry, College of Chemistry and Chemical Engineering and Innovation Laboratory for Sciences and Technologies of Energy Materials of Fujian Province (IKKEM), Xiamen University, Xiamen 361005, P. R. China.*

Changlin Tian: − *Division of Life Sciences and Medicine, University of Science and Technology of China, Hefei 230026, P. R. China;* orcid.org/0000-0001-9315-900X

Heng Yin: − *Dalian Engineering Research Center for Carbohydrate Agricultural Preparations, Dalian Technology Innovation Center for Green Agriculture, Liaoning Provincial Key Laboratory of Carbohydrates, Dalian Institute of Chemical Physics, Chinese Academy of Sciences, Dalian 116023, P. R. China;* orcid.org/0000-0001-8193-9236

Notes

The authors declare no competing financial interest.

ACKNOWLEDGMENT

This work was supported by the National Natural Science Foundation of China (22122305, 22121001, 21927814 and 22073077) and the Strategic Priority Research Program of Chinese Academy of Sciences (XDB0540000).

ABBREVIATIONS

REFERENCES

1. Harris, P. V.; Welner, D.; McFarland, K. C.; Re, E.; Poulsen, J. C. N.; Brown, K.; Salbo, R.; Ding, H. S.; Vlasenko, E.; Merino, S.; Xu, F.; Cherry, J.; Larsen, S.; Lo Leggio, L., Stimulation of lignocellulosic biomass hydrolysis by proteins of glycoside hydrolase family 61: Structure and function of a large, enigmatic family. *Biochemistry* **2010,** *49* (15), 3305-3316.

2. Vaaje-Kolstad, G.; Westereng, B.; Horn, S. J.; Liu, Z.; Zhai, H.; Sørlie, M.; Eijsink, V. G. H., An oxidative enzyme boosting the enzymatic conversion of recalcitrant polysaccharides. *Science* **2010,** *330* (6001), 219-222.

3. Solomon, E. I.; Heppner, D. E.; Johnston, E. M.; Ginsbach, J. W.; Cirera, J.; Qayyum, M.; Kieber-Emmons, M. T.; Kjaergaard, C. H.; Hadt, R. G.; Tian, L., Copper active sites in biology. *Chem. Rev.* **2014,** *114* (7), 3659-3853.

4. Munzone, A.; Eijsink, V. G. H.; Berrin, J. G.; Bissaro, B., Expanding the catalytic landscape of metalloenzymes with lytic polysaccharide monooxygenases. *Nat. Rev. Chem.* **2024,** *8* (2), 106-119.

5. Hemsworth, G. R.; Henrissat, B.; Davies G. J.; Walton, P. H., Discovery and characterization of a new family of lytic polysaccharide monooxygenases. *Nat. Chem. Biol.* **2014**, *10* (2), 122-126.

6. Frandsen, K. E. H.; Simmons, T. J.; Dupree, P.; Poulsen, J. C. N.; Hemsworth, G. R.; Ciano, L.; Johnston, E. M.; Tovborg, M.; Johansen, K. S.; von Freiesleben, P.; Marmuse, L.; Fort, S.; Cottaz, S.; Driguez, H.; Henrissat, B.; Lenfant, N.; Tuna, F.; Baldansuren, A.; Davies, G. J.; Lo Leggio, L.; Walton, P. H., The molecular basis of polysaccharide cleavage by lytic polysaccharide monooxygenases. *Nat. Chem. Biol.* **2016,** *12* (4), 298-303.

7. Quinlan, R. J.; Sweeney, M. D.; Lo Leggio, L.; Otten, H.; Poulsen, J. C. N.; Johansen, K. S.; Krogh, K. B. R. M.; Jørgensen, C. I.; Tovborg, M.; Anthonsen, A.; Tryfona, T.; Walter, C. P.; Dupree, P.; Xu, F.; Davies, G. J.; Walton, P. H., Insights into the oxidative degradation of cellulose by a copper metalloenzyme that exploits biomass components. *Proc. Natl. Acad. Sci. U.S.A.* **2011,** *108* (37), 15079-15084.

8. Sabbadin, F.; Hemsworth, G. R.; Ciano, L.; Henrissat, B.; Dupree, P.; Tryfona, T.; Marques, R. D. S.; Sweeney, S. T.; Besser, K.; Elias, L.; Pesante, G.; Li, Y.; Dowle, A. A.; Bates, R.; Gomez, L. D.; Simister, R.; Davies, G. J.; Walton, P. H.; Bruce, N. C.; McQueen-Mason, S. J., An ancient family of lytic polysaccharide monooxygenases with roles in arthropod development and biomass digestion. *Nat. Commun.* **2018,** *9* (1), 756.

9. Hemsworth, G. R.; Taylor, E. J.; Kim, R. Q.; Gregory, R. C.; Lewis, S. J.; Turkenburg, J. P.; Parkin, A.; Davies, G. J.; Walton, P. H., The copper active site of CBM33 polysaccharide oxygenases. *J. Am. Chem. Soc.* **2013,** *135* (16), 6069-6077.

10. Aachmann, F. L.; Sorlie, M.; Skjåk-Braek, G.; Eijsink, V. G. H.; Vaaje-Kolstad, G., NMR structure of a lytic polysaccharide monooxygenase provides insight into copper binding, protein dynamics, and substrate interactions. *Proc. Natl. Acad. Sci. U.S.A.* **2012,** *109* (46), 18779-18784.

11. Phillips, C. M.; Beeson, W. T.; Cate, J. H.; Marletta, M. A., Cellobiose dehydrogenaseand a copper-dependent polysaccharide monooxygenase potentiate cellulose degradation by *Neurospora crassa*. *ACS Chem. Biol.* **2011,** *6* (12), 1399-1406.

12. Munzone, A.; Pujol, M.; Tamhankar, A.; Joseph, C.; Mazurenko, I.; Réglier, M.; Jannuzzi, S. A. V.; Royant, A.; Sicoli, G.; DeBeer, S.; Orio, M.; Simaan, A. J.; Decroos, C., Integrated experimental and theoretical investigation of copper active site properties of a lytic polysaccharide monooxygenase from *Serratia marcescens*. *Inorg. Chem.* **2024,** *63* (24), 11063-11078.

13. Lim, H.; Brueggemeyer, M. T.; Transue, W. J.; Meier, K. K.; Jones, S. M.; Kroll, T.; Sokaras, D.; Kelemen, B.; Hedman, B.; Hodgson, K. O.; Solomon, E. I., Kβ X-ray emission spectroscopy of Cu(I)-lytic polysaccharide monooxygenase: direct observation of the frontier molecular orbital for H_2O_2 activation. *J. Am. Chem. Soc.* **2023,** *145* (29), 16015-16025.

14. Frandsen, K. E. H.; Tovborg, M.; Jørgensen, C. I.; Spodsberg, N.; Rosso, M. N.; Hemsworth, G. R.; Garman, E. F.; Grime, G. W.; Poulsen, J. C. N.; Batth, T. S.; Miyauchi, S.; Lipzen, A.; Daum, C.; Grigoriev, I. V.; Johansen, K. S.; Henrissat, B.; Berrin, J. G.; Lo Leggio, L., Insights into an unusual auxiliary activity 9 family member lacking the histidine brace motif of lytic polysaccharide monooxygenases. *J. Biol. Chem.* **2019,** *294* (45), 17117-17130.

15. Chaplin, A. K.; Wilson, M. T.; Hough, M. A.; Svistunenko, D. A.; Hemsworth, G. R.; Walton, P. H.; Vijgenboom, E.; Worrall, J. A. R., Heterogeneity in the histidine-brace copper coordination sphere in auxiliary activity family 10 (AA10) lytic polysaccharide monooxygenases. *J. Biol. Chem.* **2016,** *291* (24), 12838-12850.

16. Ciano L.; Davies G. J.; Tolman W. B.; Walton, P. H., Bracing copper for the catalytic oxidation of C–H bonds. *Nat. Catal.*, **2018**, *1* (8), 571-577.

17. Blanksby, S. J.; Ellison, G. B., Bond dissociation energies of organic molecules. *Acc. Chem. Res.* **2003,** *36* (4), 255-263.

18. Gao, J.; Thomas, D. A.; Sohn, C. H.; Beauchamp, J. L., Biomimetic reagents for the selective free radical and acid–base chemistry of glycans: application to glycan structure determination by mass spectrometry. *J. Am. Chem. Soc.* **2013,** *135* (29), 10684-10692.

19. Kont, R.; Bissaro, B.; Eijsink, V. G. H.; Väljamäe, P., Kinetic insights into the peroxygenase activity of cellulose-active lytic polysaccharide monooxygenases (LPMOs). *Nat. Commun.* **2020,** *11* (1), 5786.

20. Rieder, L.; Stepnov, A. A.; Sørlie, M.; Eijsink, V. G. H., Fast and specific peroxygenase reactions catalyzed by fungal mono-copper enzymes. *Biochemistry* **2021,** *60* (47), 3633-3643.

21. Chang, H.; Amengual, N. G.; Botz, A.; Schwaiger, L.; Kracher, D.; Scheiblbrandner, S.; Csarman, F.; Ludwig, R., Investigating lytic polysaccharide monooxygenase-assisted wood cell wall degradation with microsensors. *Nat. Commun.* **2022,** *13* (1), 6258.

22. Gao, W.; Li, T.; Zhou, H.; Ju, J.; Yin, H., Carbohydrate-binding modules enhance H_2O_2 tolerance by promoting lytic polysaccharide monooxygenase active site H_2O_2 consumption. *J. Biol. Chem.* **2024,** *300* (1), 105573.

23. Kuusk, S.; Bissaro, B.; Kuusk, P.; Forsberg, Z.; Eijsink, V. G. H.; Sørlie, M.; Väljamäe, P., Kinetics of H_2O_2-driven degradation of chitin by a bacterial lytic polysaccharide monooxygenase. *J. Biol. Chem.* **2018,** *293* (2), 523-531.

24. Bissaro, B.; Rohr, Å. K.; Müller, G.; Chylenski, P.; Skaugen, M.; Forsberg, Z.; Horn, S. J.; Vaaje-Kolstad, G.; Eijsink, V. G. H., Oxidative cleavage of polysaccharides by monocopper enzymes depends on H_2O_2. *Nat. Chem. Biol.* **2017,** *13* (10), 1123-1128.

25. Kim, B.; Brueggemeyer, M. T.; Transue, W. J.; Park, Y.; Cho, J.; Siegler, M. A.; Solomon, E. I.; Karlin, K. D., Fenton-like chemistry by a copper (I) complex and H_2O_2 relevant to enzyme

peroxygenase C–H hydroxylation. *J. Am. Chem. Soc.* **2023,** *145* (21), 11735-11744.
26. Caldararu, O.; Oksanen, E.; Ryde, U.; Hedegård, E. D., Mechanism of hydrogen peroxide formation by lytic polysaccharide monooxygenase. *Chem. Sci.* **2019,** *10* (2), 576-586.
27. Stepnov, A. A.; Forsberg, Z.; Sørlie, M.; Nguyen, G. S.; Wentzel, A.; Røhr, Å. K.; Eijsink, V. G. H., Unraveling the roles of the reductant and free copper ions in LPMO kinetics. *Biotechnol. Biofuels* **2021,** *14*, 28.
28. Isaksen, T.; Westereng, B.; Aachmann, F. L.; Agger, J. W.; Kracher, D.; Kittl, R.; Ludwig, R.; Haltrich, D.; Eijsink, V. G. H.; Horn, S. J., A C4-oxidizing lytic polysaccharide monooxygenase cleaving both cellulose and cello-oligosaccharides. *J. Biol. Chem.* **2014,** *289* (5), 2632-2642.
29. Hegnar, O. A.; Petrovic, D. M.; Bissaro, B.; Alfredsen, G.; Várnal, A.; Eijsink, V. G. H., pH-dependent relationship between catalytic activity and hydrogen peroxide production shown via characterization of a lytic polysaccharide monooxygenase from *Gloeophyllum trabeum*. *Appl. Environ. Microb.* **2019,** *85* (5), e02612-18.
30. Kittl, R.; Kracher, D.; Burgstaller, D.; Haltrich, D.; Ludwig, R., Production of four *Neurospora crassa* lytic polysaccharide monooxygenases in *Pichia pastoris* monitored by a fluorimetric assay. *Biotechnol. Biofuels* **2012,** *5*, 79.
31. Scott, B. R.; Huang, H. Z.; Frickman, J.; Halvorsen, R.; Johansen, K. S., Catalase improves saccharification of lignocellulose by reducing lytic polysaccharide monooxygenase-associated enzyme inactivation. *Biotechnol. Lett.* **2016,** *38* (3), 425-434.
32. Chylenski, P.; Bissaro, B.; Sørlie, M.; Røhr, Å. K.; Várnai, A.; Horn, S. J.; Eijsink, V. G. H., Lytic polysaccharide monooxygenases in enzymatic processing of lignocellulosic biomass. *ACS Catal.* **2019,** *9* (6), 4970-4991.
33. Vandhana, T. M.; Reyre, J. L.; Sushmaa, D.; Berrin, J. G.; Bissaro, B.; Madhuprakash, J., On the expansion of biological functions of lytic polysaccharide monooxygenases. *New Phytol.* **2022,** *233* (6), 2380-2396.
34. Kim, B.; Karlin, K. D., Ligand–copper (I) primary O_2-adducts: design, characterization, and biological significance of cupric–superoxides. *Acc. Chem. Res.* **2023,** *56* (16), 2197-2212.
35. Kommedal, E. G.; Sæther, F.; Hahn, T.; Eijsink, V. G. H., Natural photoredox catalysts promote light-driven lytic polysaccharide monooxygenase reactions and enzymatic turnover of biomass. *Proc. Natl. Acad. Sci. U.S.A.* **2022,** *119* (34), e2204510119.
36. Kracher, D.; Scheiblbrandner, S.; Felice, A. K. G.; Breslmayr, E.; Preims, M.; Ludwicka, K.; Haltrich, D.; Eijsink, V. G. H.; Ludwig, R., Extracellular electron transfer systems fuel cellulose oxidative degradation. *Science* **2016,** *352* (6289), 1098-1101.
37. Stepnov, A. A.; Christensen, I. A.; Forsberg, Z.; Aachmann, F. L.; Courtade, G.; Eijsink, V. G. H., The impact of reductants on the catalytic efficiency of a lytic polysaccharide monooxygenase and the special role of dehydroascorbic acid. *FEBS Lett.* **2022,** *596* (1), 53-70.
38. Momeni, M. H.; Fredslund, F.; Bissaro, B.; Raji, O.; Vuong, T. V.; Meier, S.; Nielsen, T. S.; Lombard, V.; Guigliarelli, B.; Biaso, F.; Haon, M.; Grisel, S.; Henrissat, B.; Welner, D. H.; Master, E. R.; Berrin, J. G.; Abou Hachem, M., Discovery of fungal oligosaccharide-oxidising flavo-enzymes with previously unknown substrates, redox-activity profiles and interplay with LPMOs. *Nat. Commun.* **2021,** *12* (1), 2132.
39. Kuusk, S.; Kont, R.; Kuusk, P.; Heering, A.; Sørlie, M.; Bissaro, B.; Eijsink, V. G. H.; Väljamäe, P., Kinetic insights into the role of the reductant in H_2O_2-driven degradation of chitin by a bacterial lytic polysaccharide monooxygenase. *J. Biol. Chem.* **2019,** *294* (5), 1516-1528.
40. Kuusk, S.; Eijsink, V. G. H.; Väljamäe, P., The "life-span" of lytic polysaccharide monooxygenases (LPMOs) correlates to the number of turnovers in the reductant peroxidase reaction. *J. Biol. Chem.* **2023,** *299* (9), 105094.
41. Brander, S.; Horvath, I.; Ipsen, J. Ø.; Peciulyte, A.; Olsson, L.; Hernández-Rollán, C.; Nørholm, M. H. H.; Mossin, S.; Lo Leggio, L.; Probst, C.; Thiele, D. J.; Johansen, K. S., Biochemical evidence of both copper chelation and oxygenase activity at the histidine brace. *Sci. Rep.* **2020,** *10* (1), 16369.
42. Maiti, D.; Fry, H. C.; Woertink, J. S.; Vance, M. A.; Solomon, E. I.; Karlin, K. D., A 1:1 copper−dioxygen adduct is an end-on bound super-oxo copper(II) complex which undergoes oxygenation re-actions with phenols. *J. Am. Chem. Soc.* **2007,** *129* (2), 264-265.
43. O'Dell, W. B.; Agarwal, P. K.; Meilleur, F., Oxygen activation at the active site of a fungal lytic polysaccharide monooxygenase. *Angew. Chem., Int. Ed.* **2017,** *56* (3), 767-770.
44. Tucci, F. J.; Rosenzweig, A. C., Direct methane oxidation by copper-and iron-dependent methane monooxygenases. *Chem. Rev.* **2024,** *124* (3), 1288-1320.
45. Peng, W.; Wang, Z.; Zhang, Q.; Yan, S.; Wang, B., Unraveling the valence state and reactivity of copper centers in membrane-bound particulate methane monooxygenase. *J. Am. Chem. Soc.* **2023,** *145* (46), 25304-25317.
46. Wang, B.; Zhang, X.; Fang, W.; Rovira, C.; Shaik, S., How do metalloproteins tame the Fenton reaction and utilize •OH radicals in constructive manners? *Acc. Chem. Res.* **2022,** *55* (16), 2280-2290.
47. Koo, C. W.; Tucci, F. J.; He, Y.; Rosenzweig, A. C., Recovery of particulate methane monooxygenase structure and activity in a lipid bilayer. *Science* **2022,** *375* (6586), 1287-1291.
48. Peng, W.; Qu, X.; Shaik, S.; Wang, B., Deciphering the oxygen activation mechanism at the Cu_C site of particulate methane monooxygenase. *Nat. Catal.* **2021,** *4* (4), 266-273.
49. Søndergaard, C. R.; Olsson, M. H. M.; Rostkowski, M.; Jensen, J. H., Improved treatment of ligands and coupling effects in empirical calculation and rationalization of pK_a values. *J. Chem. Theory Comput.* **2011,** *7* (7), 2284-2295.
50. Case, D. A.; Ben-Shalom, I. Y.; Brozell, S. R.; Cerutti, D. S.; Cheatham, T. E.; III, V. W. D. C.; Darden, T. A.; Duke, R. E.; Ghoreishi, D.; Gilson, M. K.; Gohlke, H.; Goetz, A. W.; Greene, D.; Harris, R.; Homeyer, N.; Izadi, S.; Kovalenko, A.; Kurtzman, T.; Lee, T. S.; LeGrand, S.; Li, P.; Lin, C.; Liu, J.; Luchko, T.; Luo, R.; Mermelstein, D. J.; Merz, K. M.; Miao, Y.; Monard, G.; Nguyen, C.; Nguyen, H.; Omelyan, I.; Onufriev, A.; Pan, F.; Qi, R.; Roe, D. R.; Roitberg, A.; Sagui, C.; Schott-Verdugo, S.; Shen, J.; Simmerling, C. L.; Smith, J.; Salomon-Ferrer, R.; Swails, J.; Walker, R. C.; Wang, J.; Wei, H.; Wolf, R. M.; Wu, X.; Xiao, L.; York, D. M.; Kollman, P. A. *AMBER 2018*; University of California: San Francisco, **2018**.
51. Li, P.; Merz, K. M., MCPB. py: A python based metal center parameter builder. *J. Chem. Inf. Model.* **2016,** *56* (4), 599-604.
52. Wang, J.; Wolf, R. M.; Caldwell, J. W.; Kollman, P. A.; Case, D. A., Development and testing of a general amber force field. *J. Comput. Chem.* **2004,** *25* (9), 1157-1174.
53. Bayly, C. I.; Cieplak, P.; Cornell, W.; Kollman, P. A., A well-behaved electrostatic potential based method using charge restraints for deriving atomic charges: the RESP model. *J. Phys. Chem.* **1993,** *97* (40), 10269-10280.
54. Metz, S.; Kästner, J.; Sokol, A. A.; Keal, T. W.; Sherwood, P., ChemShell−a modular software package for QM/MM simulations. *WIREs Comput. Mol. Sci.* **2014,** *4* (2), 101-110.
55. de Vries, A. H.; Sherwood, P.; Collins, S. J.; Rigby, A. M.; Rigutto, M.; Kramer, G. J., Zeolite structure and reactivity by combined quantum-chemical−classical calculations. *J. Phys. Chem. B.* **1999,** *103* (29), 6133-6141.

56. Furche, F.; Ahlrichs, R.; Hättig, C.; Klopper, W.; Sierka, M.; Weigend, F., Turbomole. *WIREs Comput. Mol. Sci.* **2014,** *4* (2), 91-100.
57. Smith, W.; Yong, C. W.; Rodger, P. M., DL_POLY: Application to molecular simulation. *Mol. Simul.* **2002,** *28* (5), 385-471.
58. Bakowies, D.; Thiel, W., Hybrid models for combined quantum mechanical and molecular mechanical approaches. *J. Phys. Chem. A* **1996,** *100* (25), 10580-10594.
59. Lee, C.; Yang, W.; Parr, R. G., Development of the Colle-Salvetti correlation-energy formula into a functional of the electron density. *Phys. Rev. B* **1988,** *37* (2), 785-789.
60. Becke, A. D., Density-functional thermochemistry. II. The effect of the Perdew–Wang generalized-gradient correlation correction. *J. Chem. Phys.* **1992,** *97* (12), 9173-9177.
61. Becke, A. D., Density-functional thermochemistry. III. The role of exact exchange. *J. Chem. Phys.* **1993,** *98* (7), 5648-5652.
62. Grimme, S., Semiempirical GGA-type density functional constructed with a long-range dispersion correction. *J. Comput. Chem.* **2006,** *27* (15), 1787-1799.
63. Grimme, S.; Antony, J.; Ehrlich, S.; Krieg, H., A consistent and accurate ab initio parametrization of density functional dispersion correction (DFT-D) for the 94 elements H-Pu. *J. Chem. Phys.* **2010,** *132* (15), 154104.
64. Grimme, S.; Ehrlich, S.; Goerigk, L., Effect of the damping function in dispersion corrected density functional theory. *J. Comput. Chem.* **2011,** *32* (7), 1456-1465.
65. Kästner, J.; Carr, J. M.; Keal, T. W.; Thiel, W.; Wander, A.; Sherwood, P., DL-FIND: An open-source geometry optimizer for atomistic simulations. *J. Phys. Chem. A* **2009,** *113* (43), 11856-11865.
66. Maier, J. A.; Martinez, C.; Kasavajhala, K.; Wickstrom, L.; Hauser, K. E.; Simmerling, C., ff14SB: Improving the accuracy of protein side chain and backbone parameters from ff99SB. *J. Chem. Theory Comput.* **2015,** *11* (8), 3696-3713.
67. Blomberg, M. R. A.; Borowski, T.; Himo, F.; Liao, R. Z.; Siegbahn, P. E. M., Quantum chemical studies of mechanisms for metalloenzymes. *Chem. Rev.* **2014,** *114* (7), 3601-3658.
68. Kalita, S.; Shaik, S.; Dubey, K. D., Mechanistic conundrum of C–C bond cleavage by CYP51. *ACS Catal.* **2022,** *12* (9), 5673-5683.
69. Zhou, T. P.; Feng, J.; Wang, Y.; Li, S.; Wang, B., Substrate conformational switch enables the stereoselective dimerization in P450 NascB: insights from molecular dynamics simulations and quantum mechanical/molecular mechanical calculations. *JACS Au* **2024,** *4* (4), 1591-1604.
70. Song, X.; Wang, Q.; Zhu, X.; Fang, W.; Liu, X.; Shi, C.; Chang, Z.; Jiang, H.; Wang, B., Unraveling the catalytic mechanism of taxadiene-5α-hydroxylase from crystallography and computational analyses. *ACS Catal.* **2024,** *14* (6), 3912-3925.
71. Peng, W.; Yan, S.; Zhang, X.; Liao, L.; Zhang, J.; Shaik, S.; Wang, B., How do preorganized electric fields function in catalytic cycles? The case of the enzyme tyrosine hydroxylase. *J. Am. Chem. Soc.* **2022,** *144* (44), 20484-20494.
72. Li, H.; Liu, Y., Mechanistic investigation of isonitrile formation catalyzed by the nonheme iron/α-KG-dependent decarboxylase (ScoE). *ACS Catal.* **2020,** *10* (5), 2942-2957.
73. Zhao, C.; Li, Y.; Wang, C.; Chen, H., Mechanistic dichotomy in the activation of SAM by radical SAM enzymes: QM/MM modeling deciphers the determinant. *ACS Catal.* **2020,** *10* (22), 13245-13250.
74. Senn, H. M.; Thiel, S.; Thiel, W., Enzymatic hydroxylation in *p*-hydroxybenzoate hydroxylase: a case study for QM/MM molecular dynamics. *J. Chem. Theory Comput.* **2005,** *1* (3), 494-505.
75. Ryde, U., QM/MM calculations on proteins. *Methods Enzymol.* **2016**, *577*, 119-158.
76. Zhang, Y.; Liu, H.; Yang, W., Free energy calculation on enzyme reactions with an efficient iterative procedure to determine minimum energy paths on a combined ab initio QM/MM potential energy surface. *J. Chem. Phys.* **2000,** *112* (8), 3483-3492.
77. Yue, D.; Hirao, H., Mechanism of selective aromatic hydroxylation in the metabolic transformation of paclitaxel catalyzed by human CYP3A4. *J. Chem. Inf. Model.* **2023,** *63* (24), 7826-7836.
78. Xu, K.; Hirao, H., Revisiting the catalytic mechanism of Mo–Cu carbon monoxide dehydrogenase using QM/MM and DFT calculations. *Phys. Chem. Chem. Phys.* **2018,** *20* (28), 18938-18948.
79. Neese, F., Software update: The ORCA program system—Version 5.0. *Wires Comput. Mol. Sci.* **2022,** *12* (5), e1606.
80. Humphrey, W.; Dalke, A.; Schulten, K., VMD: Visual molecular dynamics. *J. Mol. Graph. Model.* **1996,** *14* (1), 33-38.
81. Lu, T.; Chen, F., Multiwfn: A multifunctional wavefunction analyzer. *J. Comput. Chem.* **2012,** *33* (5), 580-592.
82. Haon, M.; Grisel, S.; Navarro, D.; Gruet, A.; Berrin, J. G.; Bignon, C., Recombinant protein production facility for fungal biomass-degrading enzymes using the yeast *Pichia pastoris*. *Front. Microbiol.* **2015,** *6*, 1002.
83. Brander, S.; Tokin, R.; Ipsen, J. Ø.; Jensen, P. E.; Hernández-Rollán, C.; Nørholm, M. H. H.; Lo Leggio, L.; Dupree, P.; Johansen, K. S., Scission of glucosidic bonds by a *Lentinus similis* lytic polysaccharide monooxygenases is strictly dependent on H_2O_2 while the oxidation of saccharide products depends on O_2. *ACS Catal.* **2021,** *11* (22), 13848-13859.
84. Stoll, S.; Schweiger, A., EasySpin, a comprehensive software package for spectral simulation and analysis in EPR. *J. Magn. Reson.* **2006,** *178* (1), 42-55.
85. Christensen, I. A.; Eijsink, V. G. H.; Stepnov, A. A.; Courtade, G.; Aachmann, F. L., Following the fate of lytic polysaccharide monooxygenases under oxidative conditions by NMR spectroscopy. *Biochemistry* **2023,** *62* (12), 1976-1993.
86. Davydov, R.; Herzog, A. E.; Jodts, R. J.; Karlin, K. D.; Hoffman, B. M., End-on copper(I) superoxo and Cu(II) peroxo and hydroperoxo complexes generated by cryoreduction/annealing and characterized by EPR/ENDOR spectroscopy. *J. Am. Chem. Soc.* **2022,** *144* (1), 377-389.
87. Hota, P. K.; Jose, A.; Panda, S.; Dunietz, E. M.; Herzog, A. E.; Wojcik, L.; Le Poul, N.; Belle, C.; Solomon, E. I.; Karlin, K. D., Coordination variations within binuclear copper dioxygen-derived (Hydro) peroxo and superoxo species; influences upon thermodynamic and electronic properties. *J. Am. Chem. Soc.* **2024,** *146* (19), 13066-13082.
88. Conner, K. P.; Schimpf, A. M.; Cruce, A. A.; McLean, K. J.; Munro, A. W.; Frank, D. J.; Krzyaniak, M. D.; de Montellano, P. O.; Bowman, M. K.; Atkins, W. M., Strength of axial water ligation in substrate-free cytochrome P450s is isoform dependent. *Biochemistry* **2014,** *53* (9), 1428-1434.
89. Denisov, I. G.; Makris, T. M.; Sligar, S. G.; Schlichting, I., Structure and chemistry of cytochrome P450. *Chem. Rev.* **2005,** *105* (6), 2253-2278.
90. Munro, A. W.; Girvan, H. M.; Mason, A. E.; Dunford, A. J.; McLean, K. J., What makes a P450 tick? *Trends Biochem. Sci.* **2013,** *38* (3), 140-150.
91. Whitehouse, C. J. C.; Bell, S. G.; Wong, L. L., $P450_{BM3}$ (CYP102A1): connecting the dots. *Chem. Soc. Rev.* **2012,** *41* (3), 1218-1260.
92. Hemsworth, G. R.; Ciano, L.; Davies, G. J.; Walton, P. H., Production and spectroscopic characterization of lytic polysaccharide monooxygenases. *Methods Enzymol.* **2018,** *613*, 63-90.
93. Kjaergaard, C. H.; Qayyum, M. F.; Wong, S. D.; Xu, F.; Hemsworth, G. R.; Walton, D. J.; Young, N. A.; Davies, G. J.; Walton, P. H.; Johansen, K. S.; Hodgson, K. O.; Hedman, B.; Solomon, E. I., Spectroscopic and computational insight into the activation of O_2 by the mononuclear Cu center in polysaccharide

monooxygenases. *Proc. Natl. Acad. Sci. U.S.A.* **2014,** *111* (24), 8797-8802.
94. Simmons, T. J.; Frandsen, K. E. H.; Ciano, L.; Tryfona, T.; Lenfant, N.; Poulsen, J. C.; Wilson, L. F. L.; Tandrup, T.; Tovborg, M.; Schnorr, K.; Johansen, K. S.; Henrissat, B.; Walton, P. H.; Lo Leggio, L.; Dupree, P., Structural and electronic determinants of lytic polysaccharide monooxygenase reactivity on polysaccharide substrates. *Nat. Commun.* **2017,** *8* (1), 1064.
95. Liu, Y.; Ying, Y. L.; Wang, H. Y.; Cao, C.; Li, D. W.; Zhang, W. Q.; Long, Y. T., Real-time monitoring of the oxidative response of a membrane–channel biomimetic system to free radicals. *Chem. Commun.* **2013,** *49* (59), 6584-6586.
96. Ramasarma, T.; Rao, A. V. S.; Devi, M. M.; Omkumar, R. V.; Bhagyashree, K. S.; Bhat, S. V., New insights of superoxide dismutase inhibition of pyrogallol autoxidation. *Mol. Cell. Biochem.* **2015,** *400* (1-2), 277-285.
97. Tucci, F. J.; Jodts, R. J.; Hoffman, B. M.; Rosenzweig, A. C., Product analogue binding identifies the copper active site of particulate methane monooxygenase. *Nat. Catal.* **2023,** *6* (12), 1194-1204.